AIAA SciTech
13-17 January 2014, National Harbor, Maryland
52nd Aerospace Sciences Meeting

Global Luminescent Oil-film Skin-Friction Meter Generalized to Three-Dimensional Geometry and Applied to FAITH Hill

Nicholas Husen[1]
School of Aeronautics and Astronautics
Purdue University, West Lafayette, IN 47906

Sudesh Woodiga[2], Tianshu Liu[3]
Western Michigan University, Kalamazoo, MI 49008

and

John P. Sullivan[4]
School of Aeronautics and Astronautics
Purdue University, West Lafayette, IN 47906

This paper further develops the global luminescent oil-film skin-friction meter by considering its application to a three dimensional axisymmetric wall-mounted bump subjected to subsonic turbulent boundary layer flow. The geometry gives rise to a necklace vortex and large scale separation on its lee side. An oil-film is only usable by the global luminescent oil-film skin-friction meter if it meets certain criteria. Most notably, it must be sufficiently thick to provide a good signal but not so thick that the relationship between luminescent intensity and oil-film thickness becomes nonlinear. Different regions on the model give rise to a usable oil-film at different times in an experiment. This paper proposes a technique for the selection of which solutions from a sequence of "snapshot solutions" taken during the run should be averaged for a particular region on the model. A relative skin-friction distribution resulting from the techniques proposed herein is presented for each of four sections of the model: One down the model's centerline, and three across the model in the spanwise direction.

Nomenclature

y	= height of model	g_i	= i-th component of gravity
H	= total height of model	τ_i	= i-th component of skin-friction
h	= thickness of oil film	C_{ij}	= change of coordinate matrix
r	= radial distance from origin	I	= Intensity of luminescent oil-film
(X^1, X^2, X^3)	= global coordinate system in object space	I_{ex}	= Intensity of the excitation light incident on the oil-film
$(\bar{X}^1, \bar{X}^2, \bar{X}^3)$	= coordinate system with 1-2 plane locally tangent to surface	a	= coefficient proportional to quantum efficiency of luminescent molecules
$(\tilde{X}^1, \tilde{X}^2, \tilde{X}^3)$	= coordinate system with 1-2 plane parallel with image plane	$\boldsymbol{\tau}$	= skin-friction
S	= function describing surface of model in (X^1, X^2, X^3) coordinates	$\bar{\boldsymbol{\tau}}$	= equivelant skin-friction
$\tilde{S}$	= function describing surface of model in $(\tilde{X}^1, \tilde{X}^2, \tilde{X}^3)$ coordinates	α	= Lagrange multiplier
t	= time		
p	= static pressure of external flow field		
μ	= dynamic viscosity of oil-film		
ρ	= density of oil-film		

[1] Graduate Assistant, School of Aeronautics and Astronautics, 701 West Stadium Avenue. Student Member AIAA.
[2] Graduate Assistant, Department of Mechanical and Aeronautical Engineering, Parkview Campus, MI 49008.
[3] Professor, Department of Mechanical and Aeronautical Engineering, G-220, Parkview Campus, MI 49008, Senior Member AIAA.
[4] Professor, School of Aeronautics and Astronautics, 701 West StadiumAvenue. Fellow AIAA.

I. Introduction

Aerodynamic wall shear stress, or skin friction, is one of the most important quantities in aeronautical engineering. It gives rise to a considerable portion of the drag on commercial aircraft and is used extensively by the CFD community to gleam boundary layer velocity profile information and for setting scaling parameters such as u_τ and $y+$. Many CFD practitioners are working to model turbulent flows over three dimensional geometries and find themselves without a skin friction data set against which they can validate their models or to which they can tune their models. A recent test case for CFD validation, examined by Bell et al. (2012), at NASA Ames in conjunction with AerospaceComputing, Inc., is an axisymmetric wall mounted bump, coined FAITH (Fundamental Aero Investigates The Hill) hill, subjected to subsonic turbulent boundary layer flow. Up to a scalar, the height of the geometry is defined in polar coordinates by

$$y = \cos\left(\frac{\pi}{3}r\right) + 1. \tag{1}$$

Subsonic turbulent boundary layer flow over this geometry gives rise to a rich flow field, offering for investigation massively separated regions, regions of very high and very low skin friction, and unsteady fluctuations of many kilohertz. Figure 1 shows a model of the geometry with a developed oil film on its surface and details many of the prominent surface features of this flow.

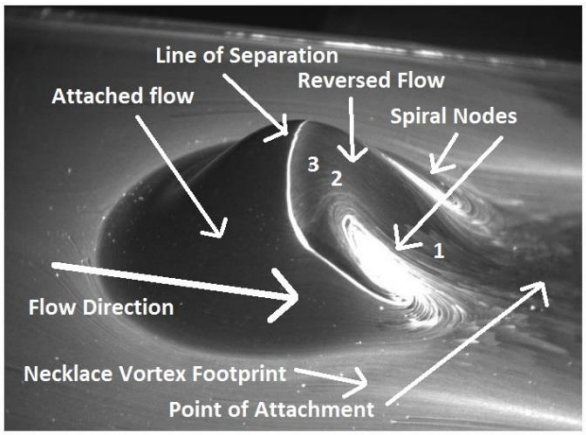

Figure 1: Image of FAITH hill with a developed oil film on its surface. Region 1: reversed flow, high magnitude skin friction, region 2: reversed flow, low magnitude skin friction, region 3: reversed flow, high magnitude skin friction—discussed in Section VI.

The present research investigates the use of a luminescent oil-film skin-friction meter to measure with unprecedented spatial resolution the shear stress on the surface of FAITH hill. The local spatial and temporal evolution of the thickness of a thin oil film provides information about the local shear stress values (both direction and magnitude) (Tanner and Blows (1976)). Brought to its current state of the art by Liu et al. (1998, 2008), the luminescent oil-film skin-friction meter uses the luminescent intensity of the oil film at a point to back out the thickness of the film at that point. This technique can quickly provide shear stress information at each of hundreds of points per square inch and is robust to many different surfaces. Other techniques require special surfaces (laser interferometer techniques) or are complicated and/or require altering the surface of the model (MEMS, liquid crystal techniques).

II. The Luminescent Skin-Friction Meter

A derivation from the Navier Stokes equations of an equation modeling the evolution of a thin oil-film under the influence of an external three-dimensional flow was presented by Brown and Naughton (1999). Allowing (X^1, X^2, X^3) to be a global coordinate system in object space, $X^3 = S(X^1, X^2)$ to be the surface defined in object space and $(\bar{X}^1, \bar{X}^2, \bar{X}^3)$ to be an orthonormal coordinate system such that $\bar{X}^1$ and $\bar{X}^2$ are locally tangent to the model's surface, the resulting "thin oil-film equation" is given by

$$\frac{\partial h}{\partial t} + \frac{\partial}{\partial \bar{X}^i}\left[\frac{\tau_i h^2}{2\mu} - \left(\frac{\partial p}{\partial \bar{X}^i} - \rho g_i\right)\frac{h^3}{3\mu}\right] = 0 \tag{2}$$

where h is the thickness of the thin oil-film, p is pressure, ρ is the density of the oil, μ is the viscosity of the oil, and g_i is the i-th component of gravity. For this analysis, the thin oil-film equation is recast in an orthonormal coordinate system denoted $(\tilde{X}^1, \tilde{X}^2, \tilde{X}^3)$ such that the $\tilde{X}^1$- $\tilde{X}^2$ plane is parallel to the image plane, where the $(\tilde{X}^1, \tilde{X}^2, \tilde{X}^3)$ coordinate vectors are determined from camera calibration (Liu (2004)). The coordinates are then transformed via

$$\tilde{X}^j = C_{ij} X^i \tag{3}$$

where

$$C_{ij} = \tilde{X}^i \cdot X^j \tag{4}$$

such that $\tilde{X}^3 = \tilde{S}(\tilde{X}^1, \tilde{X}^2)$. The thin oil-film equation is then projected onto the $\tilde{X}^1$- $\tilde{X}^2$ plane, resulting in

$$\frac{\partial h}{\partial t} + \frac{\partial}{\partial \tilde{X}^i}\left[\frac{\tau_i h^2}{2\mu} - \left(\frac{\partial p}{\partial \tilde{X}^i} - \rho g_i\right)\frac{h^3}{3\mu}\right] = 0 \tag{5}$$

The $\tilde{X}^1 - \tilde{X}^2$ plane is then projected onto the image plane. We denote the coordinates of the image plane by (x^1, x^2) and define them such that the perspective center, determined through camera calibration, is projected onto the origin of the (x^1, x^2)-coordinate system. The luminescent intensity scalar field projected onto the $\tilde{X}^1$- $\tilde{X}^2$ plane is then related to the scalar field in the image plane through $x^i = \lambda \tilde{X}^i$, where $\lambda = \lambda(\tilde{X}^1, \tilde{X}^2)$ is the ratio of the distance between the perspective center and the principle point in the image plane (the origin) and the distance from the point $(\tilde{X}^1, \tilde{X}^2, S(\tilde{X}^1, \tilde{X}^2))$ and the

plane through the perspective center parallel with the $\tilde{X}^1$- $\tilde{X}^2$ plane. For this study, λ is approximated to be a constant.

Luminescent oil film techniques capitalize on the fact that the luminescent intensity of the oil-film is directly proportional to the thickness of the oil-film (Liu and Sullivan (1998)). This linear relationship is modeled through

$$I(X^1, X^2) = a\, I_{ex}(X^1, X^2) h(X^1, X^2) \tag{6}$$

where I_{ex} is the intensity of the excitation light on the surface of the oil film, and a is a constant proportional to the quantum efficiency of the luminescent molecules in the dye and also to the concentration of these molecules in the oil. Defining g by $g = I/I_{ex}$, equation 5 can be written as

$$\frac{\partial g}{\partial t} + \lambda \frac{\partial}{\partial x^i}\left[\frac{\tau_i}{2\mu a} g^2 - \left(\lambda \frac{\partial p}{\partial x^i} - \rho g_i\right)\frac{1}{3\mu a} g^3\right] = 0 \tag{7}$$

Equation 7 is an equation for the evolution of the intensity of a luminescent thin oil-film under the influence of an external three-dimensional flow field. By introducing the "equivalent skin-friction", denoted by $\bar{\boldsymbol{\tau}}$ and defined by

$$\bar{\boldsymbol{\tau}} = \boldsymbol{\tau} g \frac{\lambda}{2\mu a} \tag{8}$$

equation 7 is rewritten as

$$\frac{\partial g}{\partial t} + \nabla(g\bar{\boldsymbol{\tau}}) = f(x_1, x_2, g) \tag{9}$$

where

$$f(x_1, x_2, g) = \lambda \frac{\partial}{\partial x_i}\left[\left(\lambda \frac{\partial p}{\partial x_i} - \rho g_i\right)\frac{g^3}{3\mu a}\right] \tag{10}$$

Equation 10 does not uniquely determine the direction of the skin-friction, and therefore does not uniquely determine the magnitude of the skin-friction, too. Ideally, at each point on the model's surface the direction of the skin-friction would be known ex-ante—then equation 10 would uniquely define the skin-friction magnitudes (Naughton and Brown (1996)). In this paper the Horn and Schunck (1981) constraint is used to close this system of equations. Although it is not physically supported, the Horn and Schunck constraint minimizes the sum of the squares of the magnitudes of the components of the gradient of the resulting equivalent skin friction vectors. This is effectively a smoothness constraint, and gives way to the following functional for minimizing $\int_\Omega (|\nabla\bar{\tau}_1|^2 + |\nabla\bar{\tau}_2|^2) dx_1 dx_2$ subject to equation 9 holding exactly.

$$J(\bar{\boldsymbol{\tau}}) = \int_\Omega \left[\frac{\partial g}{\partial t} + \nabla\cdot(g\bar{\boldsymbol{\tau}}) - f\right]^2 dx_1 dx\_2 + \alpha \int_\Omega (|\nabla\bar{\tau}_1|^2 + |\nabla\bar{\tau}_2|^2) dx_1 dx_2 \tag{11}$$

The minimization problem is reduced to the following pair of Euler-Lagrange equations through the use of Green's theorem and calculus of variations (Liu et al. (2008)).

$$\begin{aligned} g\frac{\partial}{\partial x_1}\left[\frac{\partial g}{\partial t} + \nabla\cdot(g\bar{\boldsymbol{\tau}}) - f\right] + \alpha\nabla^2\bar{\tau}_1 = 0 \\ g\frac{\partial}{\partial x_2}\left[\frac{\partial g}{\partial t} + \nabla\cdot(g\bar{\boldsymbol{\tau}}) - f\right] + \alpha\nabla^2\bar{\tau}_2 = 0 \end{aligned} \tag{12}$$

These Euler-Lagrange equations are those which are solved numerically as detailed in Liu et al. (2008). The resulting vector field is the equivalent skin friction field in the image plane. Equation 8 can be employed in order to back out the relative skin friction field, and a change of coordinates transforms the resulting shear stress vectors from $(\tilde{X}^1, \tilde{X}^2, \tilde{X}^3)$-space to (X^1, X^2, X^3)-space.

III. Measurement System

The results reported in this paper were obtained from experiments which were conducted using Dow Corning 200 5 cSt silicone oil. This oil was made to fluoresce under 450nm light by dissolving into it an oil UV tracer dye—DFSB-K175 from RiskReactor. The emission spectrum of the dye once dissolved in the silicone oil and excited by 450nm light has a local maximum around 630nm. The luminescent oil was sprayed onto the surface with an airbrush, and a 450nm LED source from LED Supply was used to excite the oil in an otherwise dark environment. A 12 bit color PCO Pixelfly QE with 1392 × 1024 pixel resolution was fitted with a 600nm low pass filter and used to record images at a rate of 5 frames per second, the timing of which was regulated by a 9600+ series delay generator from Quantum Composers.

IV. Experimental Setup

The experiments detailed herein were conducted in an open circuit wind tunnel with an open test section. The opening of the wind tunnel measured 18 inches in the spanwise direction and 12 inches vertically. The FAITH model, defined in inches and in polar coordinates by equation 1, was machined from laminated MDF, painted white with Monokote primer and finished with Krylon Crystal Clear acrylic spray paint. The model was placed 24 inches downstream from the start of the test section.

At the entrance of the test section the boundary layer was tripped with 60-grit sandpaper. The boundary layer velocity profile was measured about three model heights upstream of the center of the model using hot-wire anemometry and is provided in Figure 2. The boundary layer thickness is about one third the height of the model. This is roughly the same boundary layer thickness as was reported by Bell et al. (2012). The model was installed in the test section at the time of the measurements.

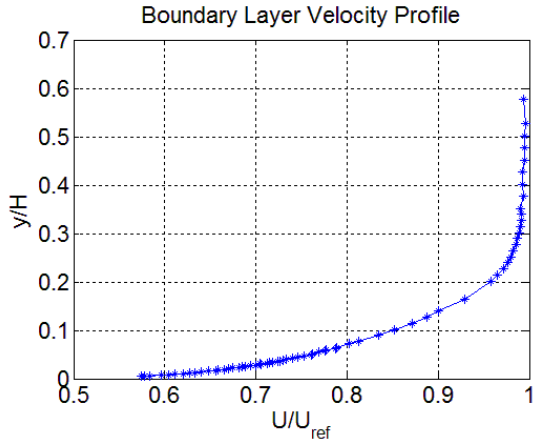

Figure 2: Hotwire traverse in boundary layer 3 model heights upstream of model center.

Before the experiment, two sequences of 100 images each were recorded without oil on the model. The first was with a 500nm high-pass optical filter. The average of this sequence of images provided the intensity levels of the excitation light which were reflected from the white surface of the model. This image was used as a proxy for the spatial variation of the excitation light incident on the model, I_{ex}. Due to the three dimensional nature of the model, the level of excitation scattered into the camera from the model's white surface had considerable spatial variation. Further, the light source is circular and does not reach to the peripheral regions of the field of view. The intensity scattered into the camera is therefore seen to become considerably less intense about one and one half hill diameters upstream of the center of the model. For this experiment the light was mounted downstream of the model and above the model at an angle of about 15 degrees from vertical. The placement of the light was a compromise between obtaining an evenly illuminated model and reducing spectral reflections of the light into the camera. The image is smoothed considerably so as to not capture strongly the physically small variations in intensity that were due to imperfections in the model's finish. Figure 3 shows the averaged image from this first sequence of images.

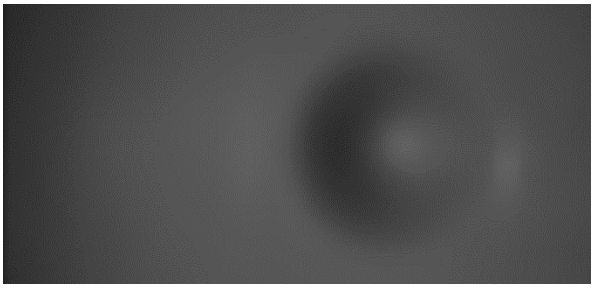

Figure 3: Image showing intensity levels of excitation light reflected from the white surface of the model.

The filter was then changed to a 550nm low-pass filter so that the excitation light was blocked and the luminescence from the oil-film was allowed to pass. The second pre-experiment sequence of images was taken. The average of this sequence provided a level of background signal which was later subtracted from each image taken during the oil-film experiment.

While monitoring a live image of the experiment from the PCO camera on a computer monitor, 5 cSt luminescent oil was then applied to the surface of the model using an airbrush. An initial oil-film thickness of about 60 microns was found to give adequate signal for a 60ms exposure time. This particularly thin oil film does not give rise to surface instabilities in the form of ripples, particularly as it is sheared away in time (Murphy, Westphal (1986)). The recording sequence was started, and the tunnel was brought to 110ft/s over 10 seconds, providing a Reynolds number based on the model's total height of $Re_H \approx 133{,}000$ and a boundary layer Reynolds number based on the distance from the start of the test section to the model's center of about $Re_x \approx 1.3 \times 10^6$.

In order to deduce a relative skin-friction field the experimenter needs for the relationship between oil-film thickness and luminescent intensity to be linear. Because the precise concentration of the dye, camera placement, and light placement vary from one experiment to the next it is important to calibrate the oil-film-luminescent intensity relationship. This calibration is done during the minutes before or after an experiment by placing a glass plate over a small amount of oil with one end of the glass plate supported by 0.005 inch shim stock. This creates a thickness distribution that is linear is space. An image sequence is taken of this oil-film distribution, and the average of that sequence is recorded. Figure 4 shows the resulting curve. Importantly, the oil-film thickness-luminescent intensity ceases to be linear when the oil is thicker than about 85 microns. Also, when linearly extrapolated back to the origin, the curve is seen to pass through the vertical axis at about 10000 counts. This is attributed to optical complications from the glass plate and to background levels of luminescence. Given the information in this plot it was determined that an upper threshold intensity of 45000 be maintained to ensure that a linear relation between luminescent intensity and oil-film thickness could be used in the numerical scheme with which the data was processed (Equation 6).

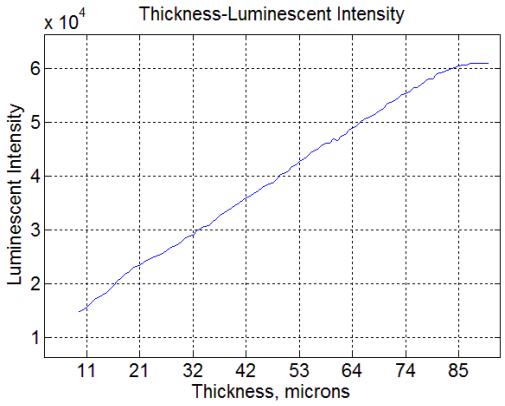

Figure 4: Curve showing luminescent intensity vs. oil-film thickness.

V. Data Processing

The execution of one experiment yields a sequence of images of the evolution of the oil film. Spatial derivatives can be numerically approximated within each image, but the approximation of temporal derivatives requires at least two images. We term one solution reduced from one pair of images as a "snapshot" solution. The problem of how to choose the pair of images for each snapshot solution (and perhaps even for each pixel) arises.

For many three-dimensional flows, and for the flow over FAITH hill in particular, the oil film evolves more rapidly in some regions of the model than it does in other regions of the model. It is therefore possible that for a particular region of interest the snapshot solution must be taken from a time in the oil-film evolution different from that for another region of interest. We can see from Figure 4 that the oil film appears to have a linear relationship with luminescent intensity for thicknesses less than about 70 microns, erring conservatively. For a particular region of interest, therefore, we are interested in the oil film evolution over a period of time during which the oil-film is sufficiently thick to provide an adequate signal-to-noise ratio but thin enough for the luminescent intensity-oil film thickness relationship to be linear. One further constraint is that the oil film be thin enough that the luminescent intensity of the oil not saturate the camera. For regions that collect oil, for example, the image pair must be taken early in the experiment. For regions of high shear, the initially applied thin oil film will be quickly sheared away. Any snapshot solution taken thereafter will offer a signal to noise ratio too small to contribute meaningfully to an average of any subset of snapshot solutions. It is evident that a process is necessary for finding for each region of interest a subset of solutions which can meaningfully be averaged.

Proposed here is a technique which follows naturally for resolving a global relative shear stress field: For each pixel, several snapshot solutions are averaged. A snapshot solution is included in the average if at the time of the snapshot solution the oil-film condition is such that (1) the oil film is thick enough to provide an adequate signal to noise ratio, and (2) the oil-film is thin enough so that the luminescent intensity-oil-film thickness relationship is linear and (3) the intensity does not saturate the camera.

The images are initially formatted as color TIFF files and are immediately converted to .mat files of double precision values representing only the red channel. This reduces the spatial resolution in each direction by a factor of two. However, the blue and green channels offer little additional information because the emission spectrum of the dye under a 450nm excitation source peaks in the red channel. The sequence of images is averaged in space and time with a $3 \times 3 \times 3$ averaging filter in Matlab, providing temporal and spatial smoothing to aleviate bit noise and noise arising from imperfect darkness in the room. At this stage the sequence is ready to be processed through the numerical scheme outlined in Section II (and detailed in the appendix of Liu et al. (2008)). This begins with inputting the quantity (the matrix) $g = I/I_{ex}$, which is a matrix of the luminescent intensities in an image of the oil-film development divided component-wise by a matrix of the luminescent intensities in the image of the excitation light distribution which was taken immediately before the experiment. The numerical scheme produces the equivalent skin friction field (equation (8)). A relative skin friction field is therefore recovered by multiplying $\bar{\boldsymbol{\tau}}$ by I_{ex}/I .

The frames used for producing the solutions which were averaged to create the figures in this article were taken after the tunnel had been running for about 40 seconds. The snapshot solutions used in this paper were computed using a Δt of one second (every fifth frame), and successive snapshot solutions used as a first frame the last frame from the previous snapshot solution. This is depicted in Figure 5.

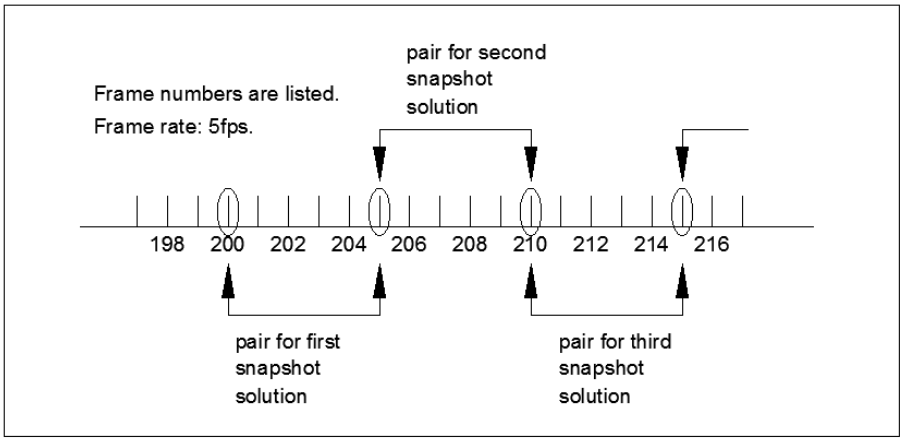

Figure 5 Schematic of which frames where used for each snapshot solution in this article.

A full set of snapshot solutions was developed, and the intensity of each pixel of each utilized image was recorded. The snapshot solutions were then averaged: for a particular pixel, the snapshot solution from a particular pair of images was included in the average if the level of intensity for that pixel in each of the two images was between particular user-defined lower and upper thresholds. The lower threshold was chosen to be 1000 and the upper threshold was chosen to be 45,000. The value 45,000 was chosen because it ensures that the oil-film is well within the range of thicknesses for which the thickness-luminescent intensity relationship is linear.

VI. Results

Qualitative data and quantitative data are presented in this section. Figures 6 and 7 show skin friction lines and equivalent skin-friction vectors produced from an earlier experiment. Behind the data in each figure is an image taken during the run. The oil appears light and the model appears dark. In Figure 6 the reversed flow under the necklace vortex

is evident, starting from the saddle point **S1** and persisting as the region of upwind pointing skin friction lines on the windward side of the model. The point of attachment after the necklace vortex, labeled with **N1**, is shown to be about one-quarter the way up the hill. The line of attachment, **L**, is fairly well resolved but misplaced to be downstream of where it should be by about one half of one hill height. Saddle point **S1** is evident, and **S2** is almost resolved. Downstream of the model, node **N2** and saddle points **S3** and **S4** are nicely resolved as well.

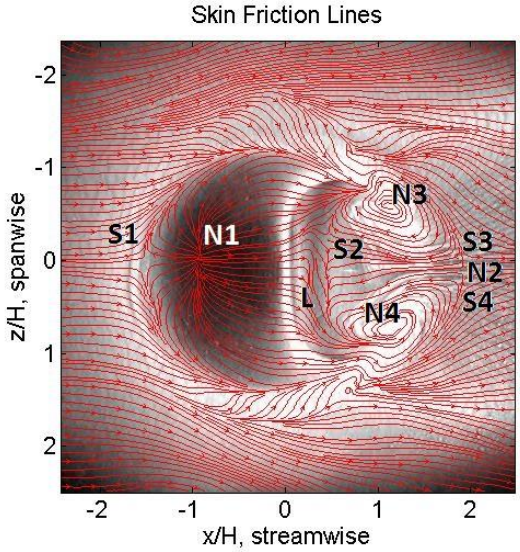

Figure 6: Skin-friction lines deduced from luminescent oil film evolution. Flow is from left to right.

The following quantitative skin friction data was deduced as per the methods detailed in earlier sections. Figure 8 is a plot of the streamwise component relative skin friction along the plane of symmetry. The experimental data from this paper is plotted together with rough approximations of the data presented as a color intensity map in Bell et al. (2012). The data were scaled so that the peak values are equal. The methodology presented in this paper reports the maximum skin friction value to occur just upstream of the model's peak, zero skin-friction in the streamwise direction is reported at the line of separation, and the skin friction values in the reversed flow region on the lee side are negative values. In the reversed flow region the skin friction has two local minima and one local maximum between those minima. This is physical. The oil film can be seen to shear upstream less aggressively at around x/H=1/2. This is observed in Figure 1. Region 1 is a region of reversed flow exhibiting high magnitude skin friction. Region 2 is a region of reversed flow but lower magnitude skin friction, and region three is a region of reversed flow with again a higher magnitude skin friction. The new data do not match the experimental data from Bell et al. The Reynolds number at which this experiment was conducted was just under one quarter of that used by Bell et al. The discrepancy between these Reynolds numbers is thought to contribute to the differences in the reported skin friction values.

Figure 9 shows the streamwise component of the relative skin-friction values along each of three spanwise cuts. Figure 10 shows the placements of those spanwise cuts. We can see that the most upstream cut is at a location with very low streamwise skin friction. It is positive in the regions on either side of the hill and at a couple of points on the surface of the model where the sectional cut emerges from being inside the necklace vortex. The spanwise cut that was close to the center of the model clearly exhibits two peaks on either side of the

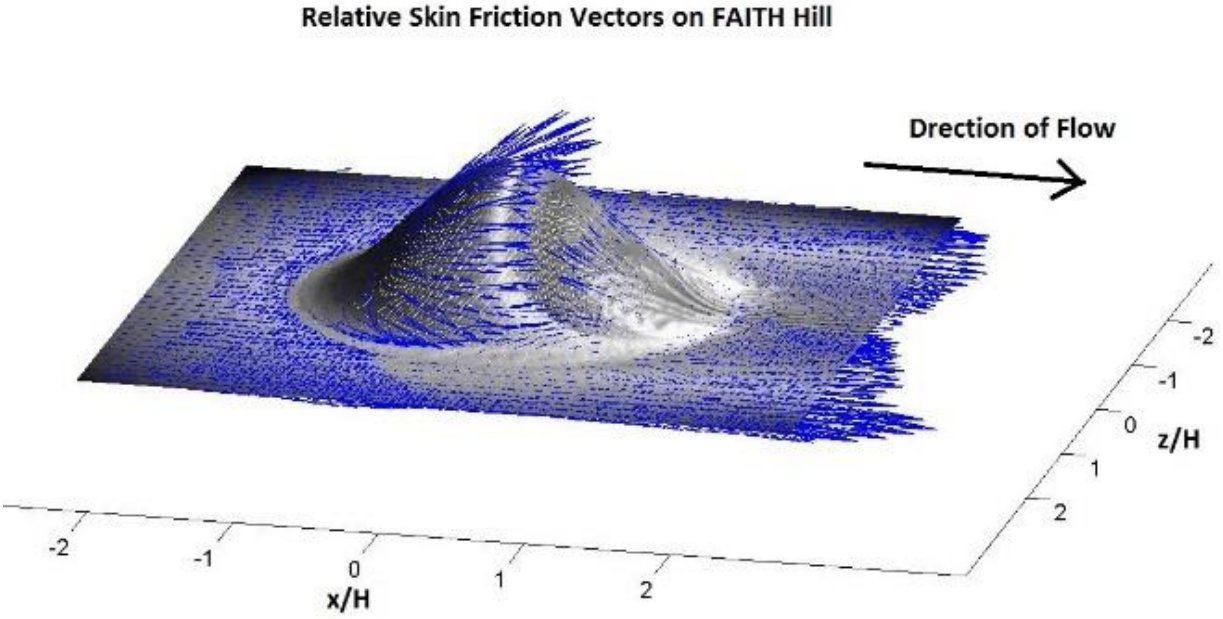

Figure 7: Relative skin friction field on the surface of FAITH hill.

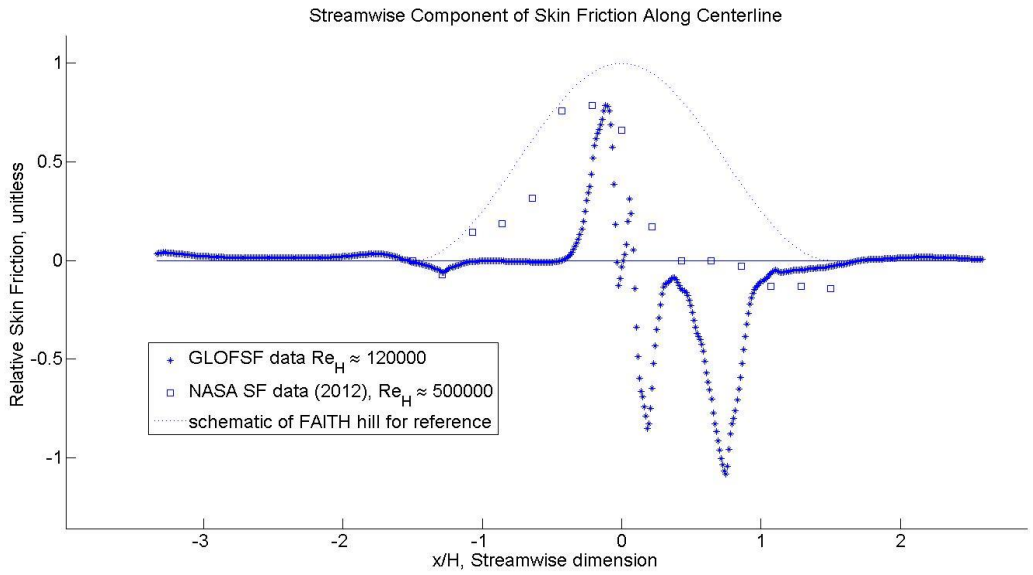

Figure 8: Streamwise component of relative skin friction along the centerline.

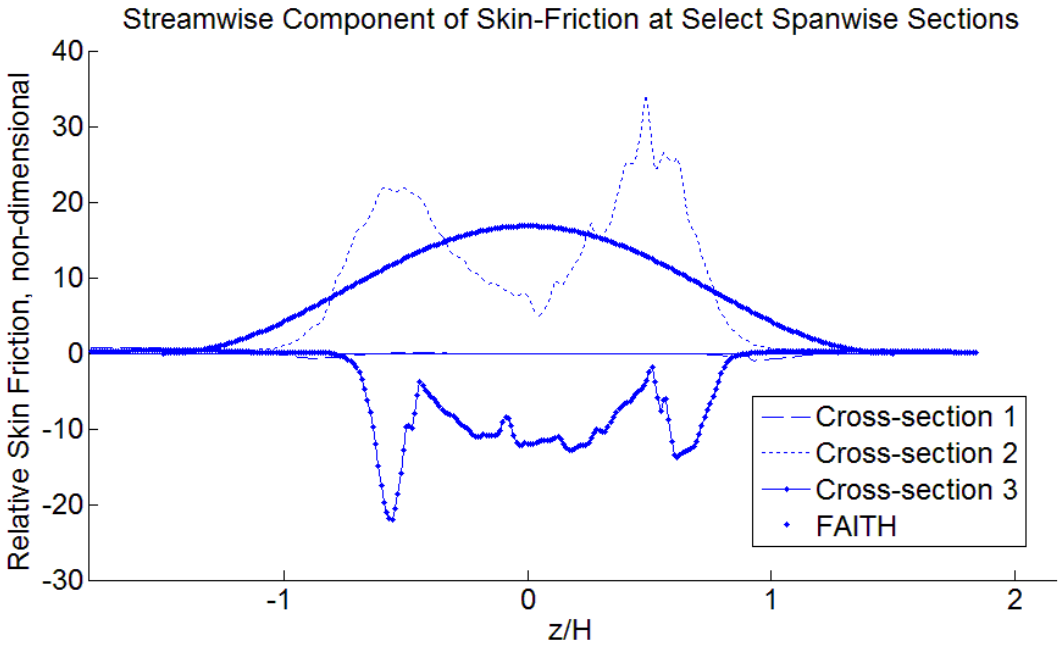

Figure 9: Streamwise skin-friction component plotted for three different spanwise sections.

model. These regions of very high skin friction are consistent with the regions shown by Bell et al. (2012) to have the highest levels of skin friction on the model.

Downstream of the model's center the streamwise component of skin friction on the model is primarily in the negative. It is most negative very near to the spiral nodes' vertices, and has a larger magnitude near the center of the model where the spanwise vortex is driving reversed flow up the lee side of the hill.

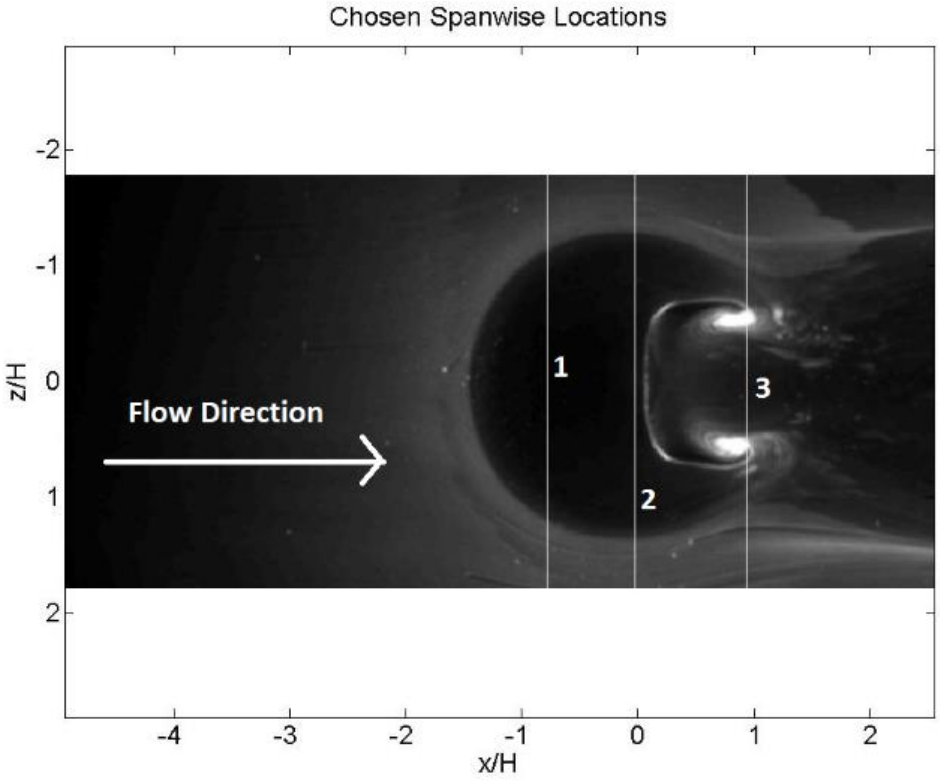

Figure 10: Locations of spanwise sections shown in figure 9.

VII. Conclusion

The prospect of obtaining quality quantitative skin friction values from the global luminescent oil-film skin friction meter is promising. Care must be taken to properly handle background levels of luminescent emission from the model's surface and to correct for uneven illumination. Further, the oil film must have certain characteristics if clean data reduction is to be performed—the oil can't be too thin or too thick, and even a thin oil-film may saturate the camera if the dye concentration is too high.

VIII. References

Brown, J. L., and Naughton, J. W., "The Thin Oil Film Equation," NASA/TM 1999-208767, March 1999

Horn, B. K., and Schunck, B. G., "Determining Optical Flow," Artificial Intelligence, Vol. 17, Nos. 1–3, 1981, pp. 185–204.

James H. Bell, James T. Heineck, Gregory Zilliac, and Rabindra D. Mehta. "Surface and Flow Field Measurements on the FAITH Hill Model," NASA Ames, 2012.

Liu, T., "Geometric and Kinematic Aspects of Image-Based Measurements of Deformable Bodies," AIAA Journal, Vol. 42, No. 9, 2004, pp. 1910–1920.

Liu, T., and Sullivan, J. P., "Luminescent Oil-Film Skin Friction Meter," AIAA Journal, Vol. 36, No. 8, 1998, pp. 1460–1465.

Liu T, Montefort J, Woodiga S, Merati P, Shen L (2008) Global luminescent oil-film skin friction meter. AIAA J 46(2):476–485

Murphy, J. D., and Westphal, R.V., "The laser Interferometer Skin-Friction Meter: A Numerical and Experimental Study," Journal of Physics E: Scientific Instruments, Vol. 19, No. 9, 1986, pp. 744-751.

Naughton, J. W., and Brown, J. L., "Surface Interferometric Skin-Friction Measurement Technique," AIAA Paper 96-2183, June 1996.

Tanner, L. H. and Blows, L. G., "A Study of the Motion of Oil Films on Surfaces in Air Flow, with Application to the Measurement of Skin Friction," Journal of Physics E: Scientific Instruments, Vol. 9, 1976, pp. 194-202.